Available online at www.ijpe-online.com

International Journal of Performability Engineering

Vol. 13, No. 4, July 2017, pp. 400-408
DOI: 10.23940/ijpe.17.04.p7.400408

Adaptive RBF Neural Network Sliding Mode Control for a DEAP Linear Actuator

Dehui Qiu[a,*], Yu Chen[a], Yuan Li[b]

[a]*College of Information Engineering, Capital Normal University, Beijing 100048, China*
[b]*School of Automation, Beijing Institute of Technology, Beijing, 100081, China*

Abstract

Dielectric electro-active polymer (DEAP) is a new smart material named "artificial muscles", which has a remarkable potential in the field of biomimetic robots. However, hysteresis nonlinearity widely exists in this material, which will reduce the performance of tracking precision and system stability. To deal with this situation, a radial basis function (RBF) neural network combined with sliding mode control algorithm is presented for a second-order DEAP linear actuator. Firstly, an inverse hysteresis operator based on Prandtl-Ishlinskii (P-I) model is used to eliminate hysteresis behavior. Secondly, an adaptive RBF neural network sliding mode controller is designed to obtain high tracking accuracy and keep system stability. The proposed algorithm makes the tracking error converge to zero and keeps the system globally stable in the case of external disturbances and parameter variations. Simulation results demonstrate that the proposed controller has the superiority to a pure sliding mode controller.

Keywords: DEAP, hysteresis; Prandtl-Ishlinskii model; RBF neural network; sliding mode control

(Submitted on January 14, 2017; Revised on May 14, 2017; Accepted on June 17, 2017)

1. Introduction

Biomimetic robots have been widely researched for several decades. A large number of research results show that biomimetic robots have vigorous vitality and huge application prospects in different kinds of fields, such as space exploration and emergency rescue. However, the robots still have obvious shortcomings in such drive mechanism and bionic material aspects [16]. There are common disadvantages in traditional drive mechanisms, including large volume, heavy mass, complicated structure and low energy consumption efficiency. The electro-active polymer (EAP) materials have similar performances to natural muscles, so they are named as "artificial muscles" [1]. This new smart drive material has a series of satisfactory features, such as low energy consumption and light mass [2]. However, hysteresis phenomenon widely exists in lots of smart material-based actuators. This situation will significantly reduce tracking precision and system stability [11]. To cope with this problem, one popular choice is characterizing the hysteresis nonlinearity by using a proper hysteresis model and then designing a certain control algorithm. Preisach model, Bouc-Wen (B-W) model, Krasnosel'skii-Pokrovkii (K-P) model, Duhem model and Prandtl-Ishlinskii (P-I) model are popular hysteresis models. The other common approach is viewing hysteresis nonlinearity as unknown disturbances and then designing suitable controller directly.

Chen and Su [4] proposed a second-order dynamic system model preceded by a P-I hysteresis representation for an ionic polymer-metal composite (IPMC) actuator, and synthesizes an adaptive model reference controller to ensure the stability of

* Corresponding author.
E-mail address: qiudehui@126.com.

the system as well as to obtain good output tracking. The shortcoming of the paper is that the uncertainties of the model are not taken into consideration. Zhang et al. [17] adopts the augmented generalized P-I model, the augmented Preisach model and the augmented linear model respectively to model the hysteresis for a supercoiled polymer (SCP) actuator, and applies open-loop position control to estimate and compensate the hysteresis effectively. Habineza et al. [6] modelled the hysteresis behavior for a piezoelectric system by using a B-W model, and compensates the hysteresis nonlinearity by using a feed-forward control approach. The common disadvantage of these two papers is that they only focus on the characterization and compensation of hysteresis, but the conclusions are not applied to a practical control objective. Rizzello et al. [14] developed various model-based feedback controllers to obtain precise tracking for a dielectric electro-active polymer (DEAP) positioning system. The paper analyzes the geometry of the DEAP membrane, but lacks time-varying characteristic. Zheng et al. [18] proposes an adaptive sliding mode controller for a DEAP actuator with hysteresis using a discrete P-I model, but the shortcoming of the paper is that there are no disturbances or uncertainties existing in the system model.

In this paper, a P-I model using play operator is used to describe the hysteresis nonlinearity for a DEAP actuator, and an inverse P-I model is used to compensate the hysteresis effect. To approximate the uncertainties in the system model and to avoid the chattering problem, an adaptive RBF neural network sliding mode controller is presented. Simulation results demonstrate that the proposed scheme has the superiority to pure sliding mode control in the existence of uncertainties for the actuator system model, including external disturbances and parameter variations.

2. Hysteresis Model of Actuators Based on Smart Materials

Nowadays, approaches of modeling hysteresis characteristic in smart materials, including electro-active polymer, shape memory alloys and so on, can be classified into two categories: physics-based models and phenomenological models [15]. Usually, the physics-based models are appropriate for specific materials, such as Duhem model and Bouc-Wen model. The phenomenological models have nothing to do with physical factors [12], such as Preisach model and Prandtl-Ishlinskii model.

The Prandtl-Ishlinskii (P-I) model has relatively simple structure compared with the Preisach model. Meanwhile, it has been proved that an inverse P-I operator in the feed-forward path can compensate the complex hysteresis behavior. So, the P-I model has been broadly adopted to denote hysteresis nonlinearity [7,10]. Both play operator and stop operator can describe the P-I model, and these two operators have complementary relationship. Thus, in this paper, the P-I model [8] is expressed by the weighted sum of play operator.

Suppose that the input $u(t)$ is a continuous function when it belongs to the time domain $[0,t_E]$. Divide the time domain $[0,t_E]$ into N subintervals, which means $0=t_0<t_1<...<t_i<...<t_N=t_E$. If the input $u(t)$ is monotone continuous on each of the subintervals, then the play operator can be defined as follows:

$$\begin{cases} P_r[u,\pi_0](0)=f_r(u(0),\pi_0) \\ P_r[u,\pi_0](t)=f_r(u(t),P_r[u,\pi_0](t_i)),t_i<t\le t_{i+1},0\le i<N-1 \\ f_r(u,w)=\max(u-r,\min(u+r,w)) \end{cases} \tag{1}$$

where $r>0$ is a threshold and π_0 is the original value of the play operator.

A simulation example of Eq. (1) is given, where $u(t)=2\sin(2\pi t)$, and the threshold is respectively equal to $r_1=2/3$ and $r_2=4/3$. Figure 1 shows the simulation result of play operator.

There are two different ways to describe the P-I model. One needs a continuous threshold; the other needs a discrete threshold. However, it is difficult to apply the P-I model using the continuous threshold to practical applications. In this paper, the latter is introduced. The P-I model using the discrete threshold can be denoted as follows:

$$H[u](t)=qu+\sum_{i=1}^{n}w_iP_{r_i}[u,\pi_0](t) \tag{2}$$

The P-I model is strictly monotonically increasing and Lipschitz continuous [7,9]. To illustrate Eq. (2), a simulation example is given, where $u(t)=20\sin(t)+20\sin(\pi t)$, $q=0.5$, $n=10$, $r_i=i$, $\pi_0\equiv 0$ and $w_i=1.5\exp(-0.03r_i)$. Figure 2 shows the simulation result of the P-I model.

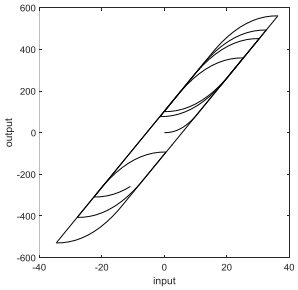

Figure 1. Play hysteresis operator

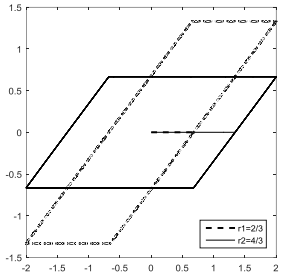

Figure 2. The Prandtl-Ishlinskii model

The form of the inverse P-I operator is the same as the P-I operator and it is Lipschitz continuous as well [8]. The formula is given as follows:

$$H^{-1}[u](t) = q^{inv}u + \sum_{i=1}^{n} w_{inv,\,i} P_{r_{inv,\,i}}[u, \pi_{inv}](t) \tag{3}$$

where

$$\begin{cases} q_{inv} = \dfrac{1}{q} \\ w_{inv,\,i} = -\dfrac{w_i}{(q + \sum_{i=1}^{j} w_j)(q + \sum_{i=1}^{j-1} w_j)} \\ r_{inv,\,i} = q r_j + \sum_{i=1}^{j-1} w_j (r_j - r_i) \\ \pi_{inv}(r_{inv,\,j}) = (q + \sum_{i=1}^{j} w_j)\pi_0(r_j) + \sum_{l=j+1}^{n} w_l \pi_0(r_l) \end{cases} \tag{4}$$

3. System Description

Dielectric electro-active polymer (DEAP), produced by Danfoss Polymer A/S, is a major kind of EAP materials. In this paper, the plant of study is a DEAP linear displacement actuator system, which can be expressed by the following dynamic second-order system [18]:

$$\begin{cases} \dot{x}_1 = x_2 \\ \dot{x}_2 = -a_1 x_1 - a_2 x_2 + w(t) + d(t) \\ w(t) = H[u](t) \\ y(t) = x_1 \end{cases} \tag{5}$$

where $u(t)$ and $y(t)$ are respectively the input and output of the system; a_1 and a_2 are uncertain parameters; $d(t)$ is the sum of external disturbances; $H[u](t)$ calculated by Eq. (2) is the hysteresis nonlinearity of the smart material. The control objective is to design an appropriate controller so that the output $y(t)$ can track the reference input $y_r(t)$ with a fast response and an accurate degree. For $y_r(t) \in C^3$, it has bounded third-order derivative.

According to [18], define $v(t) \coloneqq \hat{H}[u](t)$ to represent estimated value of $H[u](t)$. Ideally, $\hat{H}[u](t) \equiv H[u](t)$, so that $v(t) \equiv w(t)$. However, in practical situation, the error of estimation cannot be cancelled completely. Through analyzing the relationship between $H[u](t)$ and $\hat{H}[u](t)$, a conclusion can be drawn that P-I operator can be eliminated and replaced by an uncertain bounded value Δ. The definition of Δ can be seen as follows:

$$|\Delta| \le (n+1)\tilde{w}_{\max} \max\{\hat{q}_{inv}, -\sum_{i=1}^{n} \hat{w}_{inv,\,i}\} \tag{6}$$

where $(\tilde{\cdot})$ means the error of estimation and $(\hat{\cdot})$ means the estimation value with respect to the real value. By introducing the new definitions $x_3 = \dot{x}_2$ and $u_d(t) = \dot{v}(t)$, the DEAP linear displacement actuator system can be turned into:

$$\begin{cases} \dot{x}_1 = x_2 \\ \dot{x}_2 = x_3 \\ \dot{x}_3 = -a_1 x_2 - a_2 x_3 + (1+\Delta)u_d + d(t) \\ y(t) = x_1 \end{cases} \tag{7}$$

The process of reducing the hysteresis effect can be expressed by a series of cascade modules (seen in Figure 3). The modules in turn are an integrator, an inverse hysteresis operator, a hysteresis operator and a second-order linear system. The last two modules represent the whole linear displacement actuator [3,5,13].

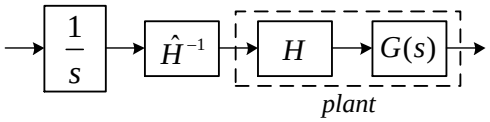

Figure 3. The DEAP system with inverse compensation

4. Design of an Adaptive RBF Neural Network Sliding Mode Controller

From the third differential equation of Eq. (7), a_1 and a_2 are uncertain parameters, so it can be rewritten as follows:

$$\begin{cases} \dot{x}_1 = x_2 \\ \dot{x}_2 = x_3 \\ \dot{x}_3 = f(x_2, x_3) + (1+\Delta)u_d + d(t) \\ y(t) = x_1 \end{cases} \tag{8}$$

where $f(\cdot)$ is a nonlinear uncertain function. When $|\Delta| \le 1$ and $|d(t)| \le D$, an adaptive RBF neural network sliding mode controller for the dynamic system is designed.

When the tracking error is equal to the reference input minus the practical output, the second derivative of the tracking error can be computed as

$$\begin{cases} e_1 = y_r - y \\ e_2 = \dot{e}_1 = \dot{y}_r - x_2 \\ e_3 = \dot{e}_2 = \ddot{y}_r - x_3 \end{cases} \tag{9}$$

Suppose that the sliding mode surface is denoted as follows:

$$s = \sigma_1 e_1 + \sigma_2 e_2 + e_3 \tag{10}$$

To ensure $p^2 + \sigma_2 p + \sigma_1$ is a Hurwitz polynomial, σ_1 and σ_2 should meet the requirement: $\sigma_2 = \alpha^2, \sigma_1 = 2\alpha, \alpha > 0$. So, the first-order derivative of s is

$$\begin{aligned} \dot{s} &= \sigma_1 \dot{e}_1 + \sigma_2 \dot{e}_2 + \dot{e}_3 \\ &= \sigma_1 \dot{e}_1 + \sigma_2 \dot{e}_2 + \ddot{y}_r - f - (1+\Delta)u_d - d(t) \end{aligned} \tag{11}$$

If $f(\cdot)$ is known, supposing $\dot{s} = 0$, then it can be obtained that

$$u_d = \frac{1}{1+\Delta}(\ddot{y}_r - f + \sigma_1 \dot{e}_1 + \sigma_2 \dot{e}_2 + \eta \,\mathrm{sgn}(s) + ks), \eta > 0, k > 0 \tag{12}$$

Substituting Eq. (12) into Eq. (11), then it can be obtained that

$$\begin{aligned} \dot{s} &= \sigma_1 \dot{e}_1 + \sigma_2 \dot{e}_2 + \ddot{y}_r - f - \ddot{y}_r + f - \sigma_1 \dot{e}_1 - \sigma_2 \dot{e}_2 - \eta \,\mathrm{sgn}(s) - ks - d(t) \\ &= -\eta \,\mathrm{sgn}(s) - ks - d(t) \end{aligned} \tag{13}$$

If $\eta \geq D$, then $s\dot{s} = -\eta|s| - sd(t) - ks^2 \leq 0$.

However, $f(\cdot)$ is an uncertain term. Neural Network is capable to approximate any continuous function to arbitrary precision, which can estimate the uncertain term $f(\cdot)$. Back Propagation(BP) neural network and Radial Basis Function (RBF) neural network are typical representatives of forward network. Compared with BP neural network, RBF neural network has simpler structure and faster learning algorithms. Thus, in this paper, RBF neural network is used to approximate the uncertain function in the system model. Figure 4 shows the schematic of adaptive control system based on RBF neural network.

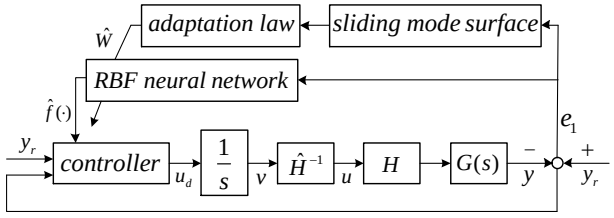

Figure 4. The schematic of adaptive control system based on RBF neural network

In this case, the RBF neural network algorithm is as follows:

$$\begin{cases} x = [e_1 e_2 e_3]^T \\ h_j = \exp(-\dfrac{\|x - c_j\|^2}{2b_j^2}),\ j = 1,2,...,5 \\ c = [c_{11}, \cdots, c_{15};\ c_{21}, \cdots, c_{25};\ c_{31} \cdots c_{35}] \\ b = [b_1, b_2, \cdots, b_5]^T \\ \hat{W} = [\hat{w}_1, \hat{w}_2, \cdots, \hat{w}_5]^T \\ \hat{f}(x) = \hat{W}^T h(x) \end{cases} \tag{14}$$

where the vector x is the input of the network, $h(x)$ is the Gaussian function, $\hat{W}$ is estimation of the weight value and $\hat{f}(x)$ is the output of the network. Figure 5 shows the structure of RBF neural network.

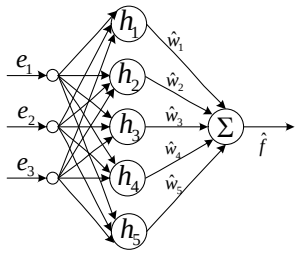

Figure 5. The structure of RBF neural network

Suppose that $\bar{W}$ is the ideal weight value vector and $\varepsilon \leq \varepsilon_N$ is the estimated error of the network, then the ideal output is as follows:

$$f = \bar{W}^T h(x) + \varepsilon \tag{15}$$

Substituting Eq. (14) into Eq. (12), it can be obtained that

$$u_d = \frac{1}{1+\Delta}(\ddot{y}_r - \hat{f} + \sigma_1 \dot{e}_1 + \sigma_2 \dot{e}_2 + \eta \,\mathrm{sgn}(s) + ks),\ \eta > 0,\ k > 0 \tag{16}$$

Substituting Eq. (15) into Eq. (13), it can be obtained that

$$\begin{aligned}\dot{s} &= \sigma_1\dot{e}_1 + \sigma_2\dot{e}_2 + \ddot{y}_r - f - \ddot{y}_r + \hat{f} - \sigma_1\dot{e}_1 - \sigma_2\dot{e}_2 - \eta\,\mathrm{sgn}(s) - ks - d(t) \\ &= -f + \hat{f} - \eta\,\mathrm{sgn}(s) - ks - d(t) \\ &= -\tilde{f} - \eta\,\mathrm{sgn}(s) - ks - d(t)\end{aligned} \tag{17}$$

where $\tilde{f} = f - \hat{f} = \bar{W}^T h(x) + \varepsilon - \hat{W}^T h(x) = \tilde{W}^T h(x) + \varepsilon$ and $\tilde{W} = \bar{W} - \hat{W}$.

Define that the Lyapunov function is $V = \frac{1}{2}s^2 + \frac{1}{2}\beta\tilde{W}^T\tilde{W},\ \beta > 0$, then the first-order derivative of V is

$$\begin{aligned}\dot{V} &= s\dot{s} + \beta\tilde{W}^T\dot{\tilde{W}} \\ &= s(-\tilde{f} - d(t) - \eta\,\mathrm{sgn}(s) - ks) - \beta\tilde{W}^T\dot{\hat{W}} \\ &= s(-\tilde{W}^T h(x) - \varepsilon - d(t) - \eta\,\mathrm{sgn}(s) - ks) - \beta\tilde{W}^T\dot{\hat{W}} \\ &= -\tilde{W}^T(sh(x) + \beta\dot{\hat{W}}) - s(\varepsilon + d(t) + \eta\,\mathrm{sgn}(s) + ks)\end{aligned} \tag{18}$$

Suppose that the adaptation law of the weight value is

$$\dot{\hat{W}} = -\frac{1}{\beta}sh(x) \tag{19}$$

Substituting Eq. (19) to Eq. (18), it can be obtained that

$$\begin{aligned}\dot{V} &= -s(\varepsilon + d(t) + \eta\,\mathrm{sgn}(s) + ks) \\ &= -s(\varepsilon + d(t)) - \eta|s| - ks^2\end{aligned} \tag{20}$$

When the estimated error ε is small enough, supposing $\eta \geq \varepsilon_N + D$, then it can be proved that $\dot{V} \leq 0$. In conclusion, the system is asymptotically stable.

5. Simulation Results

Let us consider the dynamic second-order system as follows:

$$\begin{cases}\dot{x}_1 = x_2 \\ \dot{x}_2 = -a_1x_1 - a_2x_2 + w(t) + d(t) \\ w(t) = H[u](t) \\ y(t) = x_1\end{cases} \tag{5}$$

According to Ref. (Zheng et al., 2015), the parameters of the hysteresis behavior H are: $q = 3, \tilde{w}_{\max} = 0.1$, $[w_1, w_2, \cdots, w_{10}] = [1.6375, 1.3406, 1.0976, 0.8987, 0.7358, 0.6024, 0.4932, 0.4086, 0.3306, 0.2707]$, and $[\hat{w}_1, \hat{w}_2, \cdots, \hat{w}_{10}] = [1.7004, 1.4218, 1.0230, 0.9813, 0.7622, 0.5219, 0.4489, 0.4132, 0.4221, 0.3636]$, then the inverse operator of P-I model can be computed through Eq. (3) and Eq. (4). The "input-hidden-output" structure of RBF neural network is "3-5-1", and the parameters are: $b = [15;15;15;15;15]^T$ and $c = [-1,-0.5,0,0.5,1;-1,-0.5,0,0.5,1;-1,-0.5,0,0.5,1]$. The reference input is: $y_r(t) = \sin(t)$. The parameters of the sliding mode surface s are: $\sigma_1 = 100$ and $\sigma_2 = 20$. a_1 and a_2 are uncertain parameters, but the limitations are known. In the adaptive RBF neural network control combined with sliding mode control (ARBFSMC) algorithm proposed in this paper, Eq. (16) is used as the control law and Eq. (19) is used as the adaptive law of the RBF neural network weight value.

To show the advantages of ARBFSMC algorithm, the results are compared with pure sliding mode control (SMC) algorithm. The simulation can be classified into two different situations. In the first situation, suppose that a_1 and a_2 are known constants, and takes the external disturbances into consideration, where $d(t) = 0.5\sin(t)$. In the second situation, suppose that the uncertain parameters a_1 and a_2 are time-varying, where they can be denoted as the products of constants and variable coefficients, the coefficients are $0.2\sin(t)$ and $0.2\sin(t)$ respectively. The following figures display specific simulation results.

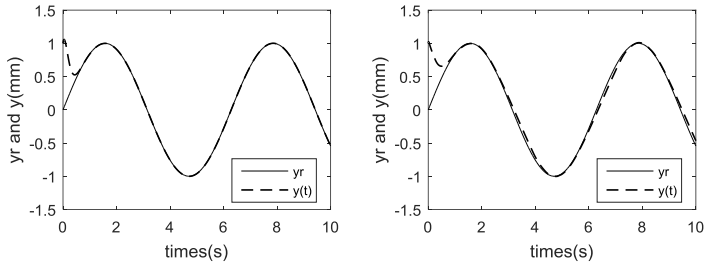

(a) ARBFSMC algorithm (b) SMC algorithm

Figure 6. Sine wave with external disturbances

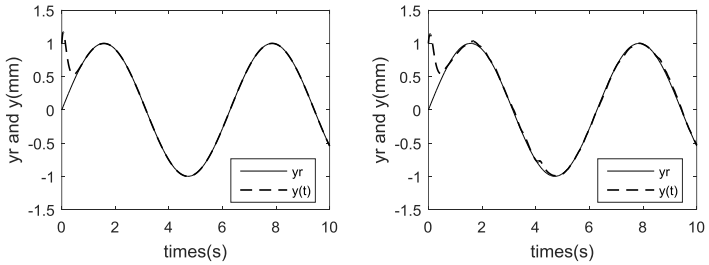

(a) ARBFSMC algorithm (b) SMC algorithm

Figure 7. Sine wave with parameter variations

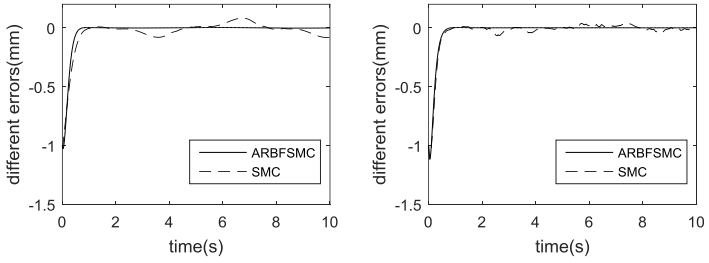

(a) external disturbances (b) parameter variations

Figure 8. Sine wave error comparisons

Figure 6 and Figure 7 show the results with external disturbances and parameter variations. Figure 8 shows the error comparisons of ARBFSMC algorithm and SMC algorithm. It can be easily found that ARBFSMC algorithm has better tracking performance than SMC algorithm in the case of disturbances and parameter variations.

Table 1. Quantitative analysis of error comparisons

Conditions \ Algorithms		ARBFSMC algorithm error (mm)	SMC algorithm error (mm)
External Disturbances $d(t)$	$0.2\sin(t)$	0.0265	0.0490
	$0.5\sin(t)$	0.0265	0.0510
Parameter Variations *coefficients of* a_1 *and* a_2	$0.1\sin(t);0.1\sin(t)$	0.0276	0.0436
	$0.2\sin(t);0.2\sin(t)$	0.0276	0.0473

In order to evaluate the tracking performance of two control methods, the average value of error is quantitatively analyzed shown in Tab. 1. As can be seen in Tab. 1, the following phenomena can be found. When the disturbances and coefficients of parameters become bigger, the error of ARBFSMC algorithm is the same as the former value. When the error of SMC algorithm becomes bigger when the uncertainties are more terrible. So the proposed algorithm has good robustness to resist external disturbances and parameter variations.

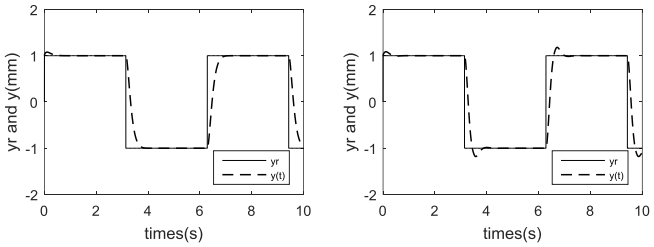

(a) ARBFSMC algorithm (b) SMC algorithm

Figure 9. Square wave with external disturbances

To prove the advantages of ARBFSMC algorithm from another aspect, make a square wave as the given input, whose amplitude is limited between $[-1,1]$. The external disturbance is $d(t)=0.5\sin(t)$, the coefficients of a_1 and a_2 are $0.2\sin(t)$ and $0.2\sin(t)$ respectively. The simulation consequences are as follows.

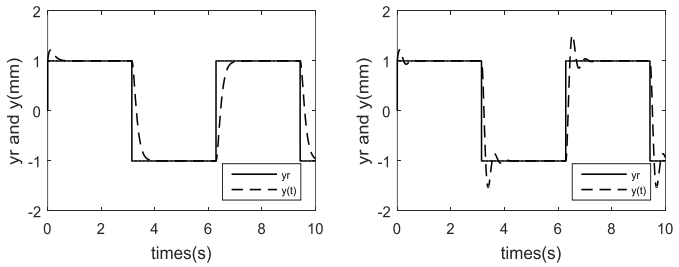

(a) ARBFSMC algorithm (b) SMC algorithm

Figure 10. Square wave with parameter variations

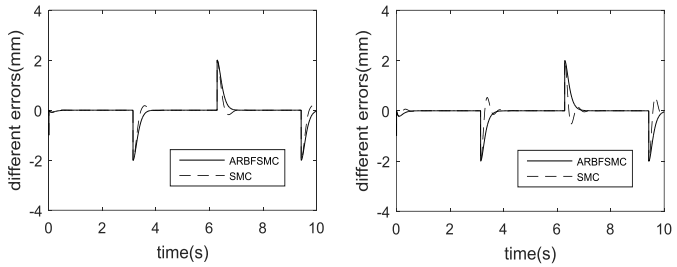

(a) external disturbances (b) parameter variations

Figure 11: Square wave error comparisons

When it comes to square wave, Figure 9 shows the results with external disturbances, Figure 10 shows the results with parameter variations, and Figure 11 shows the error comparisons. It can also be found that ARBFSMC algorithm has better tracking accuracy because its tracking error is close to zero in the existence of two different conditions. Obviously, SMC algorithm exists chattering when the system has parameter variations.

6. Conclusion

In this paper, a P-I model using a discrete threshold and play operator is adopted to describe the hysteresis characteristic of a DEAP second-order linear actuator. At the same time, an inverse operator is used to compensate the hysteresis nonlinearity. To approximate the uncertain function in the system model and to avoid the chattering phenomenon, an adaptive RBF neural network sliding mode controller is designed. The adaptive law of the RBF neural network weight value computed by the Lyapunov function ensures the stability of the system. Compared with SMC algorithm, it is obvious that the proposed ARBFSMC algorithm in this paper has better tracking accuracy because the tracking error is close to zero under the circumstance of external disturbances and parameter variations respectively. At the same time, there is no chattering behavior in the tracking process. So, the proposed control algorithm has the effectiveness of the system model with uncertainties, including disturbances and time-varying parameters. The future research will focus on enhancing the response speed and obtaining good tracking performance for a revolute-joint DEAP actuator.

Acknowledgements

This paper was supported by the National Science Foundation of China (61375100) and the general project of Beijing Municipal Commission of Education (KM201510028014).

References

1. Bar-Cohen, Y., "Biologically Inspired Intelligent Robots using Artificial Muscles", *Strain*, vol. 5051, no. 1, pp.19-24, 2003.
2. Chen, H., Wang, Y., Sheng, J., Chang, L., Wang, Y., "Research of Electro-active Polymer and Its Application in Actuators", *Chinese Journal of Mechanical Engineering*, vol. 49, no. 6, pp. 205-214, 2013.
3. Chen, X., Hisayama, T., "Adaptive Sliding-mode Position Control for Piezo-actuated Stage", *IEEE Transactions on Industrial Electronics*, vol. 55, no. 11, pp. 3927-3934, 2008.
4. Chen, X., Su, C. Y., "Adaptive Control for Ionic Polymer-Metal Composite Actuators", IEEE Transactions on Systems, Man, and Cybernetics: Systems, vol. 46, no. 10, pp. 1468-1477, 2016.

5. Edardar, M., Tan, X., Khalil, H. K., "Sliding-mode Tracking Control of Piezo-actuated Nanopositioners", in *Proceedings of American Control Conference*, pp. 3825-3830, 2012.
6. Habineza, D., Rakotondrabe, M., Gorrec, Y. L., "Bouc-Wen Modeling and Feedforward Control of Multivariable Hysteresis in Piezoelectric Systems: Application to a 3-DoF Piezotube Scanner", *IEEE Transactions on Control Systems Technology*, vol. 23, no. 5, pp. 1797-1806, 2015.
7. Krejci, P., Kuhnen, K., "Existence, Uniqueness and L∞-Stability of the Prandtl-Ishlinskii Hysteresis and Creep Compensator", *European Journal of Control*, vol. 14, no. 5, pp. 409-417, 2008.
8. Krejci, P., Kuhnen, K., "Inverse Control of Systems with Hysteresis and Creep", in *Proceedings of Conf. on Control Theory and Applications*, pp. 185-192, 2001.
9. Kuhnen, K., "*Modeling, Identification and Compensation of Complex Hysteretic Nonlinearities: A Modified Prandtl-Ishlinskii Approach*", *European Journal of Control*, vol. 9, no. 9, pp. 407-418, 2003.
10. Lian, J. W., Chen, H. Y., "Feedforward and Feedback Control for Piezoelectric-actuated Systems using Inverse Prandtl-Ishlinskii Model and Particle Swarm Optimization", in *Proceedings of Conf. on Advanced Mechatronic Systems*, pp.313-318, 2014.
11. Main, J. A., Garcia, E., "Piezoelectric Stack Actuators and Control System Design: Strategies and Pitfalls", *Journal of Guidance Control Dynamics*, vol. 20, no. 3, pp. 479-485, 2012.
12. Mayergoyz, I. D., "Mathematical Models of Hysteresis", *Physical Review Letters*, vol. 22, no. 5, pp. 603-608, 1986.
13. Riccardi, L., Naso, D., Turchiano, B., Janocha, H., "On PID Control of Dynamic Systems with Hysteresis using a Prandtl-Ishlinskii Model", in *Proceedings of American Control Conference*, pp. 1670-1675, 2012.
14. Rizzello, G., Naso, D., York, A., Seelecke, S., "Modeling, Identification, and Control of a Dielectric Electro-Active Polymer Positioning System", *IEEE Transactions on Control Systems Technology*, vol. 23, no. 2, pp. 632-643, 2015.
15. Song, Z., Long, Y., Sun, J., "General on Modeling and Control of Hysteresis Nonlinear System", *Journal of Naval Aeronautical and Astronautical University*, vol. 29, no. 6, pp. 528-534, 2014.
16. Wang, G., Chen, D., Chen, K., Zhang, Z., "The Current Research Status and Development Strategy on Biomimetic Robot", *Journal of Mechanical Engineering*, vol. 51, no. 13, pp. 27-44, 2015.
17. Zhang, J., Iyer, K., Simeonov, A., Yip, M. C., "Modeling and Inverse Compensation of Hysteresis in Supercoiled Polymer Artificial Muscles", *IEEE Robotics and Automation Letters*, vol. 2, no. 2, pp. 773-780, 2017.
18. Zheng, J., Wang, Q., Li, Y., "Adaptive Sliding Model Control for Linear Actuator with Hysteresis using a Prandtl-Ishlinskii Model", in *Proceedings* of *Conf. on Robotics and Biomimetics*, pp. 2553-2557, 2015.